Supplement of

Intra-seasonal surface velocity variability of Universidad Glacier, Central Andes of Chile (34° S), from Sentinel-1 SAR offset tracking: a two-season baseline and comparison with multi-annual velocity products

Christopher Ulloa, Ayon García, Hans Fernández-Navarro, Jorge Berkhoff, José Luis Rodriguez, Pierre Pitte

Correspondence to: christopher.ulloa@uda.cl

Contents: Sections S1 (directional-filter methodology) and S2 (station–ERA5-Land offset), Figures S1–S10 and Table S1. Data sources and processing steps are described in the main text (Sect. 3); figure captions are self-contained. All figures and tables listed above are included in this version.

Section S1. Directional post-processing filter: detailed methodology

To reduce false-positive matches commonly associated with SAR offset tracking, a directional post-processing filter constrained by glacier topography and flow geometry was applied to the displacement vectors, together with a spatial mask restricting the field to the glacier's mapped outline. The directional filter was specifically designed to correct unrealistic vector orientations detected in low-velocity sectors of the upper glacier, where image correlation is more susceptible to noise and false matches. First, a smoothed downslope flow direction was derived from the ALOS PALSAR 12.5 m DEM by calculating the local elevation gradient over a Gaussian-smoothed surface in order to suppress pixel-scale topographic noise. Second, the large-scale glacier flow geometry was represented using a manually derived glacier centerline, from which local along-flow directions were estimated. Both components were combined into a hybrid directional field representing the expected glacier flow orientation. The original offset-tracking vectors were then compared against this hybrid directional field, and vectors showing large angular deviations (>25–40° depending on glacier sector) were progressively corrected toward the expected down-glacier direction using a circular angular interpolation; no vector was discarded on the basis of this angular criterion alone. Separately, the vector field was clipped to the glacier's mapped outline to remove vectors located outside the ice margin; for the illustrative 06–18 March 2025 pair shown in Fig. S4, this outline mask reduced the vector count from 621 (full processing domain, including off-glacier terrain) to 181 (on-glacier only). The orientation correction was applied preferentially in the upper and upper-middle glacier, while vectors associated with the highest flow velocities in the glacier tongue were preserved unchanged in order to retain the original flow structure resolved by the offset-tracking algorithm. This combined procedure substantially reduced directional artifacts and produced spatially coherent velocity vector fields consistent with glacier geometry and valley topography (Fig. S4). Unless otherwise stated, all glacier-wide means, along-flow profiles and zone-specific statistics reported in the main text use the raw, unfiltered offset-tracking magnitude rasters; the directional and outline filtering described here was applied only to the illustrative vector-field figures (main-text Fig. 6, and Fig. S4). The overall processing workflow is summarised in Fig. S3.

Section S2. Station–ERA5-Land temperature offset: elevation explanation

The station sits at 2463 m a.s.l. (UTM 375541 E, 6157306 N), whereas the glacierized catchment over which ERA5-Land is effectively averaged has a DEM-derived mean elevation of 3388 m a.s.l. (median 3470 m; 154.2 km², ALOS PALSAR 12.5 m DEM). This 925 m elevation difference, combined with a standard environmental lapse rate of 6.5 °C km^{-1}, predicts a temperature difference of ≈6.0 °C, accounting for the large majority of the observed 6.8 °C offset (main text Sect. 4.6); the residual (~0.8 °C) is consistent with ERA5-Land's own smoothed model orography differing from the true terrain-derived mean elevation, and with additional exposure effects at the station site.

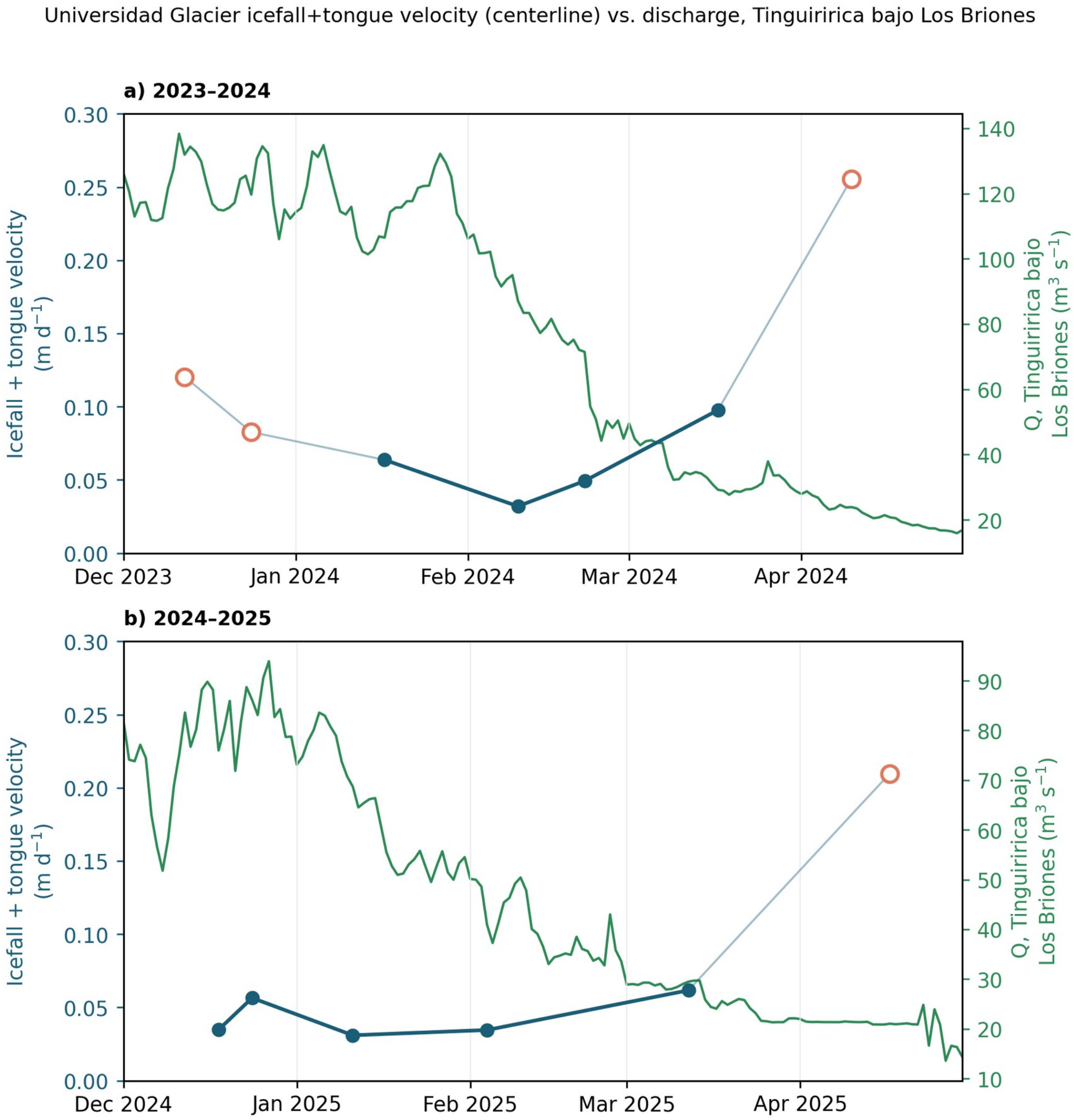

Figure S1. Icefall and tongue mean surface velocity from Sentinel-1 offset tracking (dark blue; centerline points beyond 3 km, LOWESS-smoothed, as in Fig. 9 of the main text) compared with daily mean discharge at the Tinguiririca bajo Los Briones gauge (green, right axis), for (a) the 2023–2024 and (b) the 2024–2025 ablation seasons. Discharge follows a smooth recession from a December maximum to an April minimum in both seasons, with no pulse, step or inflection coincident with the velocity changes. Seasonal mean discharge was ~39% lower in 2024–2025 (45.9 m³ s⁻¹) than in 2023–2024 (74.9 m³ s⁻¹), reflecting basin-wide precipitation and snowpack differences. Open circles mark the four pairs treated as unconfirmed pending pair-specific quality assessment (06–18 and 18–30 December 2023, 04–16 April 2024 and 11–23 April 2025; Sect. 4.1).

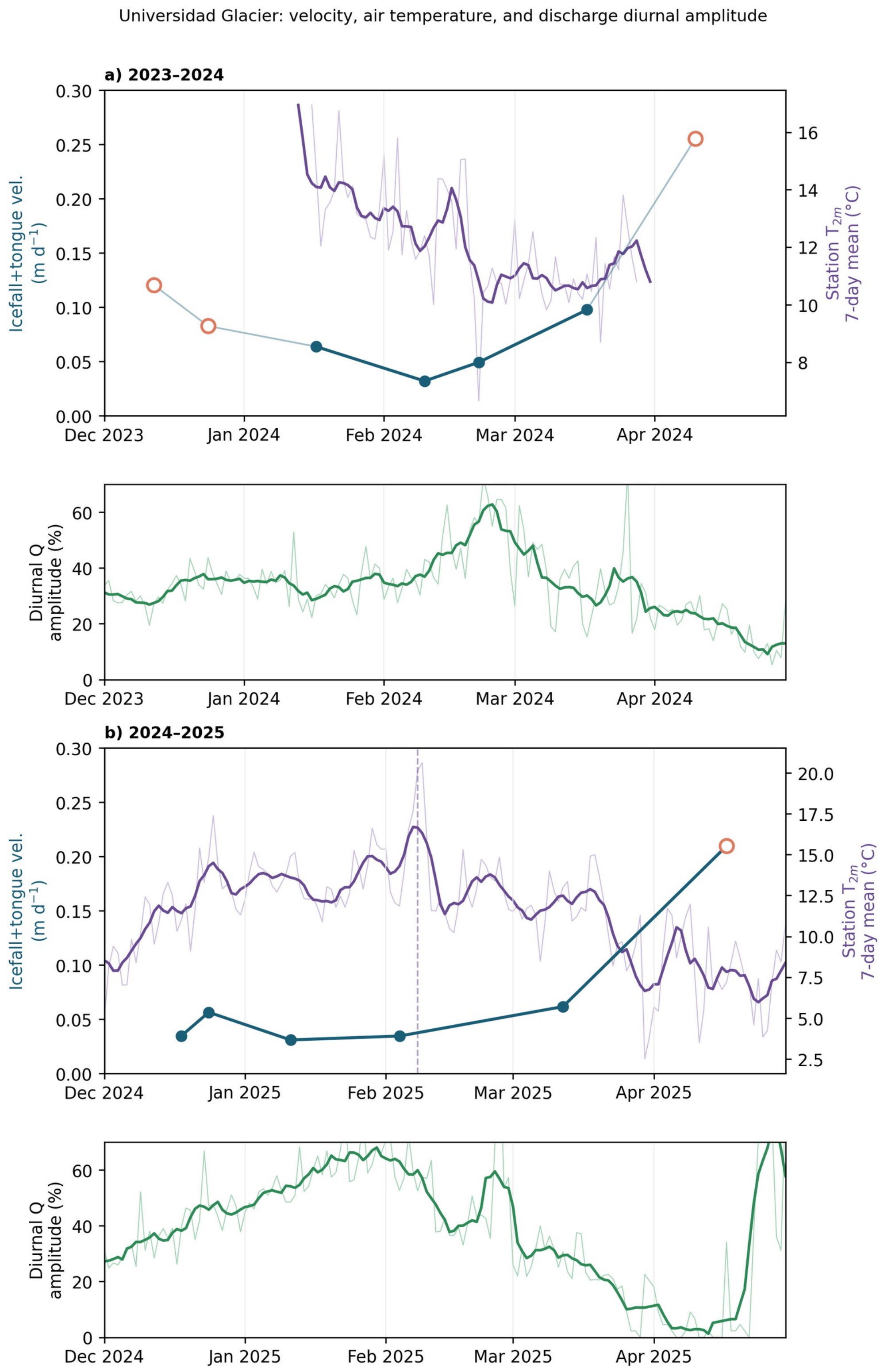

Figure S2. Icefall and tongue velocity (centerline points beyond 3 km, LOWESS-smoothed, as in Fig. 9 of the main text) and 7-day mean air temperature (upper panels; station 06023000-5 in purple, ERA5-Land in orange where the station was offline) alongside the diurnal amplitude of discharge at the Tinguiririca bajo Los Briones gauge (lower panels), for (a) 2023–2024 and (b) 2024–2025. The diurnal amplitude is the daily maximum minus minimum of the despiked 30-minute record (median filter, threshold 2.5 × the 24-hour rolling median), expressed as a percentage of the daily mean (thin line: daily values; thick line: 7-day mean). Mean amplitudes of 33–42% indicate a melt-dominated regime; the seasonal maximum (62% in 2024–2025, 55% in 2023–2024) coincides with the seasonal air-temperature maximum (dashed line in b: 8 February 2025). The noisier late-April values reflect the sensitivity of a percentage metric to small absolute discharge at base flow.

Figure S3. Workflow of the methodology (Sect. 3 of the main text): Sentinel-1 GRD pairs are DEM-assisted co-registered and processed by offset tracking in ESA SNAP (128 × 128 px window, oversampling 16, 200 m grid), directionally filtered, and sampled along the glacier centerline and at the stake locations; the GNSS stake network provides the independent velocity comparison (Sect. 4.3), and the off-glacier velocity distributions provide the empirical detection threshold (Sect. 4.4).

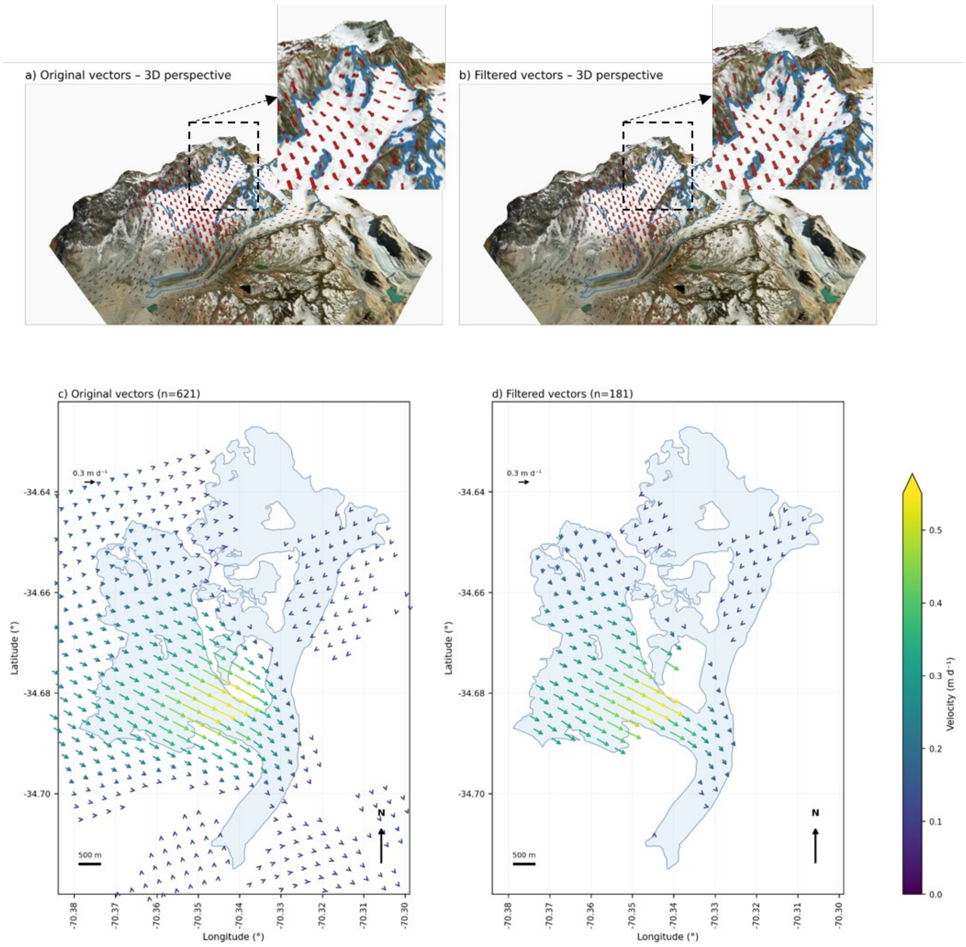

Figure S4. Effect of the directional post-processing filter (Sect. 3.1 of the main text) for the 06–18 March 2025 pair. Original (a, c) and filtered (b, d) velocity vector fields; (a, b) 3D perspective views over the ALOS PALSAR 12.5 m DEM, (c, d) plan views with arrows scaled by velocity magnitude (colour scale in m d^{-1}; scale bar 500 m). Panels (b, d) show the field after both the directional orientation correction (Sect. 3.1; applied mainly in the low-velocity upper glacier and discarding no vectors by itself) and clipping to the glacier's mapped outline (which removes off-glacier vectors and reduces the count from 621, full processing domain, to 181, on-glacier only); the high-velocity icefall and tongue vectors are unchanged by either step.

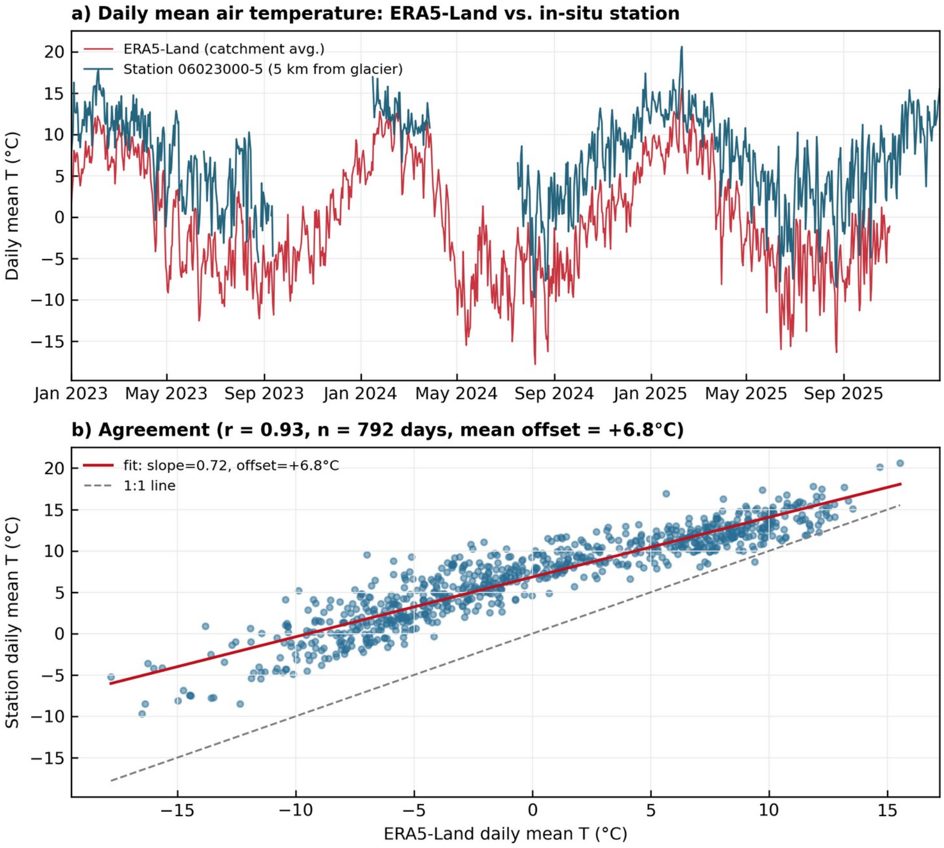

Figure S5. Agreement between the two air-temperature sources used in Sect. 4.6 of the main text. (a) Daily mean 2 m air temperature from ERA5-Land (catchment average) and from DGA station 06023000-5 (in situ, ~5 km from the glacier margin) over their full common record (November 2022 onward; station outages in October–December 2023 and April–June 2024). (b) Daily means on days with coincident data (n = 792): r = 0.93, with a systematic +6.8 °C offset (station warmer), consistent with the station's lower elevation relative to the ERA5-Land catchment average. The offset does not affect the timing analysis of the main text, which relies on relative temperature.

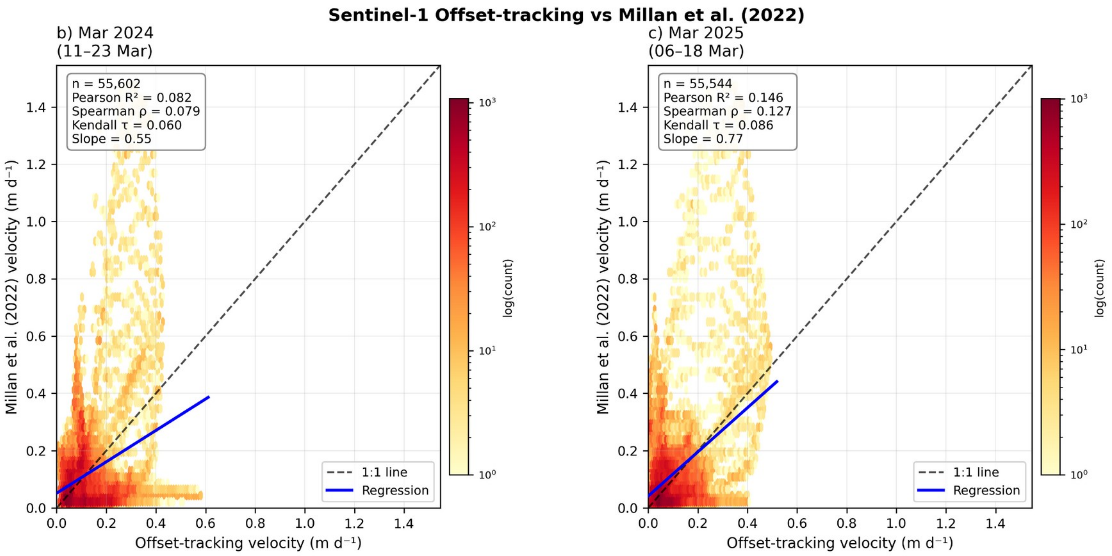

Figure S6. Density comparison (hexbin, logarithmic colour scale) between Sentinel-1 offset-tracking velocities and the 2017–2018 velocity field of Millan et al. (2022), resampled to a common grid, for (a) the 11–23 March 2024 pair (n = 55,602 pixels; Spearman ρ = 0.079, Kendall τ = 0.060, regression slope 0.55) and (b) the 06–18 March 2025 pair (n = 55,544; ρ = 0.127, τ = 0.086, slope 0.77). Dashed line: 1:1; blue line: linear regression of Millan et al. velocities on offset-tracking velocities. Because the 200 m offset-tracking grid was resampled, the number of independent samples is closer to ~600, and the very small p-values are not evidence of a strong relationship. The Millan et al. velocities exceed the offset-tracking velocities over most of the glacier (points above the 1:1 line), reflecting both the lower velocities of 2024–2025 relative to 2017–2018 and the spatial smoothing of the offset-tracking configuration (Sect. 5.1 and 5.4 of the main text). The isolated Millan et al. values reaching 1.2–1.4 m d⁻¹, well above the ~0.85 m d⁻¹ centerline peak reported in Fig. 6, occur off the digitized centerline, chiefly in the marginal shear zones and the smaller tributary branches not sampled by the along-flow profile, and are included here because the hexbin compares the full resampled grids; a small number of these may also reflect residual artifacts in the Millan et al. (2022) product rather than real ice motion.

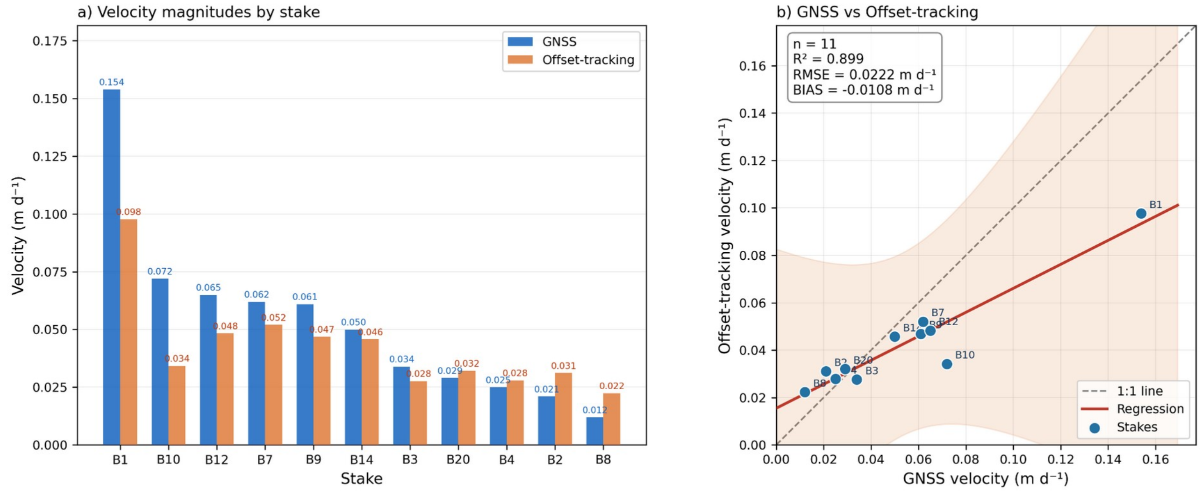

Figure S7. Surface velocity fields, 2023–2024 ablation season (all 7 pairs), clipped to the glacier outline

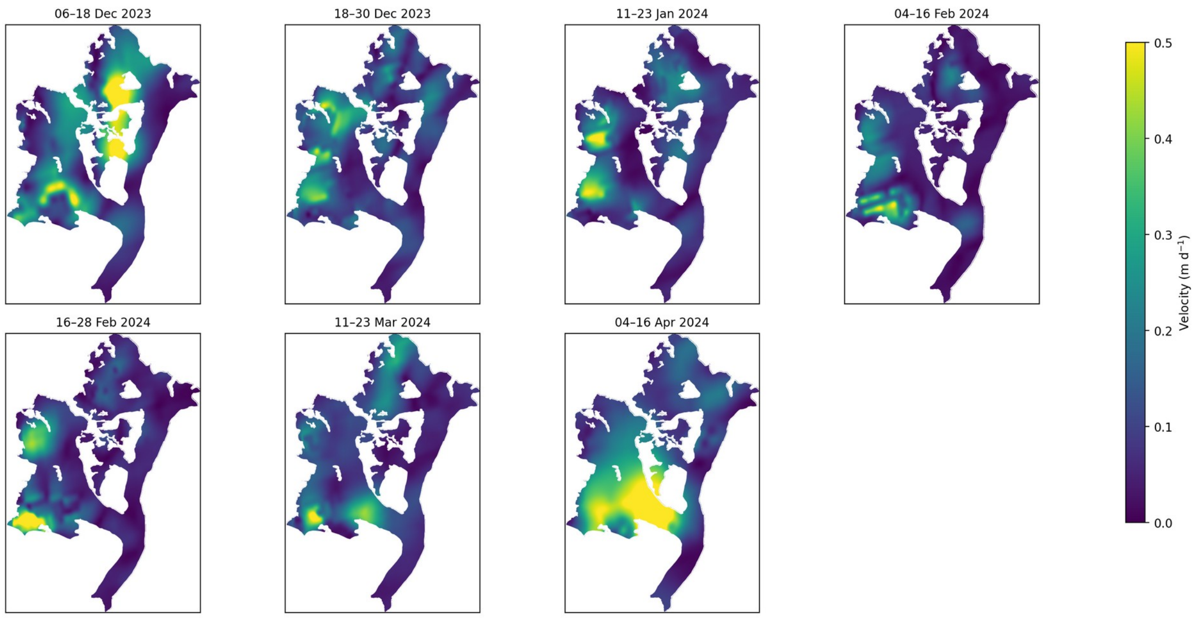

Figure S7. Surface velocity fields for all seven 2023–2024 pairs (06–18 Dec 2023 to 04–16 Apr 2024; Table 2 of the main text), clipped to the glacier outline; same colour scale as Fig. 3 of the main text. Raw, unfiltered offset-tracking rasters (Sect. 3.1). The 04–16 April 2024 panel shows the broadest high-velocity patch of the season, consistent with the icefall-zone signal-to-noise analysis in Table S1.

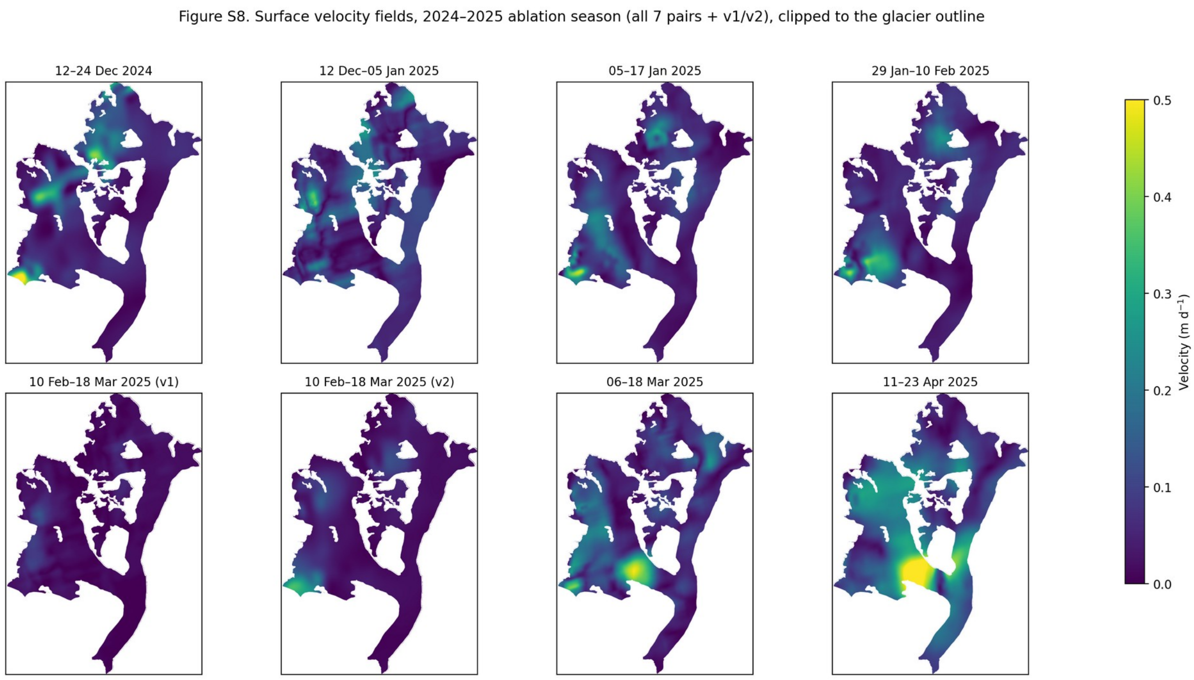

Figure S8. Surface velocity fields for all seven 2024–2025 pairs (12–24 Dec 2024 to 11–23 Apr 2025, including both v1/v2 solutions for the 10 Feb–18 Mar interval; Table 2 of the main text), clipped to the glacier outline; same colour scale as Fig. 4 of the main text. Raw, unfiltered offset-tracking rasters. The 11–23 April 2025 panel shows a more spatially confined high-velocity patch than 04–16 April 2024 (Fig. S7), though with a lower icefall-zone signal-to-noise ratio (Table S1).

Season	Pair	Off-glac. median	Off-glac. P90	Off-glac. P95	Icefall P90	Icefall/noise ratio	Note
2023-24	06–18 Dec 2023	0.016	0.089	0.116	0.264	2.28	icefall/upper-zone ratio 0.68; flagged as unconfirmed (Sect. 4.1)
2023-24	18–30 Dec 2023	0.013	0.097	0.129	0.142	1.10	icefall/upper-zone ratio 0.35; flagged as unconfirmed (Sect. 4.1)
2023-24	11–23 Jan 2024	0.012	0.081	0.100	0.118	1.18	icefall/upper-zone ratio 0.74
2023-24	04–16 Feb 2024	0.010	0.056	0.067	0.055	0.82	icefall/upper-zone ratio 0.62
2023-24	16–28 Feb 2024	0.013	0.072	0.086	0.105	1.22	icefall/upper-zone ratio 0.55
2023-24	11–23 Mar 2024	0.022	0.087	0.108	0.296	2.74	icefall/upper-zone ratio 1.41
2023-24	04–16 Apr 2024	0.022	0.130	0.173	0.820	4.75	Highest icefall/noise ratio; icefall/upper-zone ratio 2.75; flagged as unconfirmed; elevated glacier-wide, coldest conditions of season (Sect. 4.1)
2024-25	12–24 Dec 2024	0.015	0.061	0.076	0.063	0.82	icefall/upper-zone ratio 0.76
2024-25	12 Dec 2024–	0.000	0.077	0.106	0.116	1.09	icefall/upper-

	05 Jan 2025						zone ratio 0.88
2024-25	05–17 Jan 2025	0.024	0.079	0.103	0.101	0.98	icefall/upper-zone ratio 0.65
2024-25	29 Jan–10 Feb 2025	0.029	0.069	0.078	0.081	1.04	icefall/upper-zone ratio 0.63
2024-25	10 Feb–18 Mar 2025 (v1)	0.000	0.019	0.024	0.022	0.91	Ratio ≈1, not usable quantitatively; icefall/upper-zone ratio 0.56
2024-25	10 Feb–18 Mar 2025 (v2)	0.006	0.026	0.033	0.030	0.92	Ratio ≈1, not usable quantitatively; icefall/upper-zone ratio 0.35
2024-25	06–18 Mar 2025	0.008	0.057	0.071	0.316	4.43	icefall/upper-zone ratio 2.31
2024-25	11–23 Apr 2025	0.040	0.151	0.191	0.515	2.69	Elevated noise; icefall/upper-zone ratio 1.17; flagged as unconfirmed (Sect. 4.1)

Table S1. Per-pair off-glacier velocity statistics (median, 90th and 95th percentile of stable-terrain pixels, m d^{-1}) and icefall-zone (3,000–3,500 m a.s.l., DEM-based) 90th percentile, for each Sentinel-1 pair in Table 2 of the main text. The icefall/noise ratio (icefall P90 ÷ off-glacier P95) is the objective criterion discussed in Sect. 4.1 and 4.4: values above ~1 indicate a detectable signal above the stable-terrain noise floor. The Note column also reports, for each pair, the ratio of the icefall-zone (3–5 km along the centerline) to the upper-zone (0–1.5 km) mean velocity, the within-glacier criterion discussed in Sect. 4.1: values below 1 in December–February indicate the icefall signal does not exceed the upper glacier, whereas values above 1 in March and April indicate a spatially localized increase at the icefall. Rows shaded in orange flag pairs discussed individually in the main text (the two April pairs, and the two v1/v2 solutions for the 36-day 10 Feb–18 Mar 2025 interval, which have a ratio ≈ 1 and should not be used quantitatively).

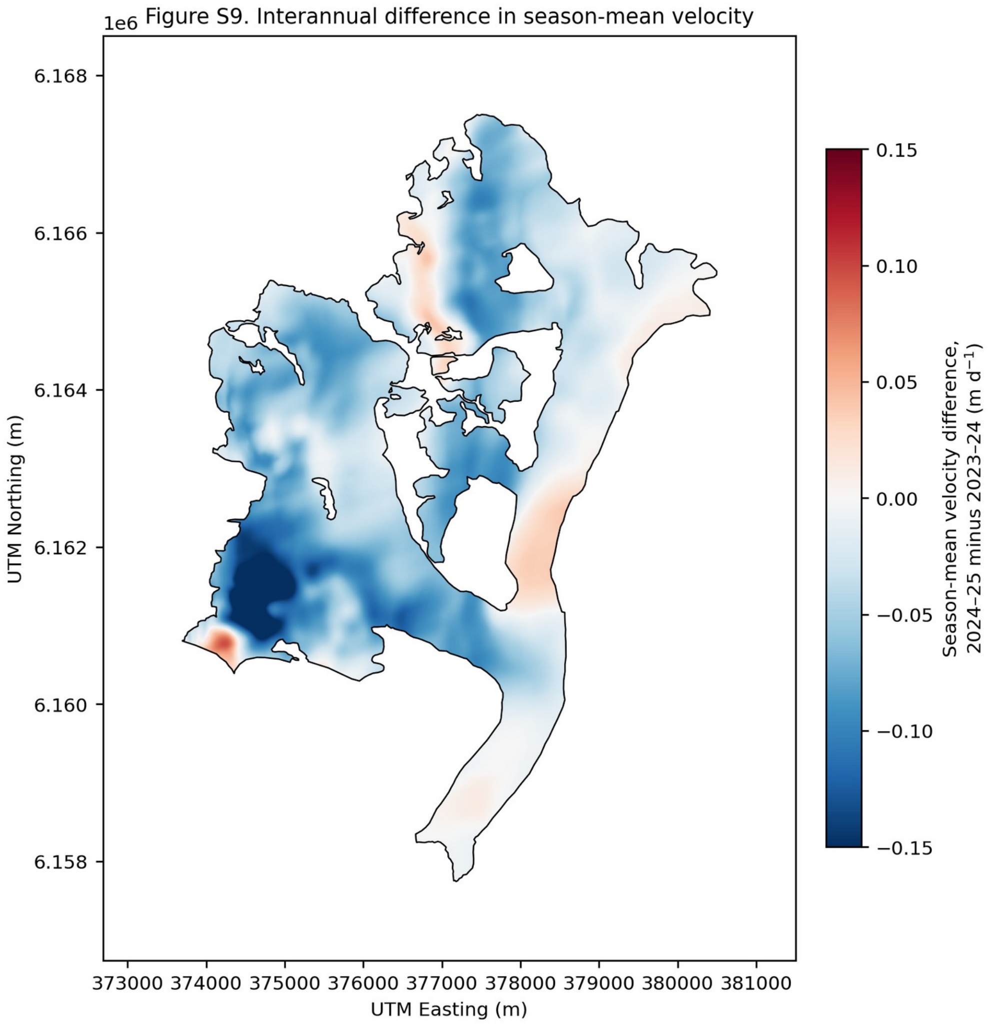

Figure S9. Pixel-wise difference in season-mean surface velocity, 2024–2025 minus 2023–2024 (raw, unfiltered rasters, on-glacier pixels only), referenced in Sect. 4.2 of the main text. The largest decrease (down to −0.25 m d^{-1}) occurs in the upper/western tributary cirque, not in the icefall or tongue; icefall and lower-tongue differences range from −0.13 to +0.04 m d^{-1} (mean −0.02), and the upper zone as a whole ranges from −0.25 to +0.10 m d^{-1} (mean −0.05), both outside the ±0.05 m d^{-1} noise level in places. Because the strongest decrease is located where the December 2023 pairs show their anomalously high values (Sect. 4.1), it is most likely dominated by those pairs rather than by a dynamic change. No value approaching +0.24 m d^{-1} is found anywhere on the glacier (maximum +0.10 m d^{-1}).

Figure S10. Field survey and stake installation on Universidad Glacier, 2024–2025 GNSS campaign. (a) GNSS receiver on tripod set up on stable ground for base-station/differential positioning, with the glacier tongue and icefall in the background. (b) View across the upper glacier surface toward the icefall. (c) Field team preparing equipment on the glacier surface, with surrounding peaks including the prominent rock tower visible in the background. (d) A team member with GNSS rover pole and ice axe standing beside a marked ablation stake location on the glacier surface. (e, f) Installation of an ablation stake: drilling into the ice with an ice axe and hand auger and inserting the stake, with the GNSS rover pole and backpack-mounted equipment alongside.